

Received February 15, 2020; reviewed; accepted June 12, 2020

Flotation separation of rutile from almandine using octadecyl amine polyoxyethylene ether as collector

Hongqiang Li¹, Huifang Zheng², Qian Chen², Richard M. Kasomo², Jiahao Leng³, Xiaoqing Weng⁴, Shaoxian Song², Linbo Xiao⁴, Chengtao Tian⁴

¹School of Resource and Safety Engineering, Wuhan Institute of Technology, Wuhan 430205, China

²College of Resource and Environmental Engineering, Wuhan University of Technology, Wuhan 430070, China

³College of Resources, Environment and Safety Engineering, Hunan University of Science and Technology, Xiangtan, 411201, China

⁴Hubei Sanning Chemical co. LTD, Yichang, 443200, China

Corresponding authors: 18378303024@163.com (H. Zheng), sxx851215@whut.edu.cn (S. Song)

Abstract: In this study, the flotation separation of rutile from almandine using cationic surfactant Octadecyl amine polyoxyethylene ether (AC1815) as a new collector was investigated. The adsorption mechanism of AC1815 on rutile was illustrated through zeta potential measurement, infrared spectrum and XPS analyses. The flotation experiments demonstrated that AC1815 exhibited an excellent collecting ability and selectivity for rutile. The results of zeta potential measurements and XPS analysis indicated that more AC1815 was adsorbed on rutile surface instead of almandine. The adsorption mechanism of AC1815 on rutile was mainly attributed to the electrostatic interaction between the positively charged molecules of AC1815 and the negatively charged rutile surface, and the hydrogen bonding between the protonated $\equiv\text{NH}^+$, $\equiv\text{N}$ group of AC1815 and Ti-OH on rutile surface.

Keywords: rutile, almandine, flotation separation, adsorption mechanism

1. Introduction

Titanium (Ti) is a very important strategic metal with extensive application, such as aviation, aerospace, navigation, machinery, medicine, chemical industry, seawater desalination (Fang et al., 2018). Rutile (TiO_2) is the main source of titanium. Hard rock rutile ores account for the large part of total reserve of rutile resources in China (Bulatovic et al., 1999). Due to the complex in their mineral composition, the concentration of hard rock rutile ores is very complex. The main beneficiation methods of rutile usually include flotation, gravity, magnetic and electrostatic separation (Abouzeid et al., 1979, Cui et al., 2002). Since the mineralogical properties of rocks are very complex, the production cost of rutile rock is high, thus, it cannot be exploited and utilized industrially. Almandine ($\text{Fe}_3\text{Al}_2(\text{SiO}_4)_3$) is the main gangue mineral in hard rock rutile ores. The density and specific susceptibility of almandine are close to that of rutile, consequently, flotation is considered to be an efficient method to separate rutile from almandine (Xu et al., 2017, Chen et al., 2018). Many collectors have been applied in rutile flotation, such as fatty acids (Xiao et al., 2019), various soaps of vegetable oils, and petroleum sulphonate (Liu et al., 1999). The main challenge of these collectors is the lack of selectivity and specificity for gangue minerals, such as apatite and almandine among others (Xie et al., 2018). For example, flotation study to extract rutile valuable minerals from copper tailings slurry was conducted using soluble petroleum sulfonate as the rutile collector and hydrofluoric acid as the depressant, respectively. Low grade concentrate assaying 34.8% TiO_2 was obtained from a feed containing 0.76% TiO_2 (Xu et al., 2017). Nonyl hydroxamic acid (Wang et al., 2016), arsenic acids, phosphonic acids (Liu et al., 1999), N-benzoyl-N-phenylhydroxylamine (N-BPHA), alkyl succinamates (Bulatovic et al., 1999), and 3,4-(methylenedioxy) benzyl acrylate acid also have been tried in the flotation of rutile ores (Bertiniet al., 1991, Liet al., 2016). Celik et

al. (1998) used the hydroxamate as the collector to remove titanium minerals such as rutile and sphene from a Turkish feldspar ore. The results clearly demonstrated that hydroxamate exhibited better performance than fatty acids (Celiket et al., 1998). In application of hydroxamate was used as collector in rutile flotation, heavy metal ions Pb^{2+} must be added as an activator although that may cause serious environmental pollution. Cui et al. (1986) used benzyl arsonic acid (BAA) as a rutile collector, sodium fluorosilicate (Na_2SiF_6) as a gangue depressant, and a rutile concentrate assaying 84.5% TiO_2 was produced with the flotation recovery of 86.4% (Cui, et al., 1986). The flow-sheet and reagent scheme from this study were employed in the Zaoyang Rutile Mine, China. However, the Zaoyang Rutile Mine had to be closed because of the high reagent cost and the environmental concerns (Liu et al., 1999). Phosphonic acids have proven to be highly selective collector for flotation recovery of rutile under weakly acidic condition, with less toxicity than benzyl arsenic acid (BAA). However, the high reagent consumption of the expensive phosphonic acids limits its industrial application.

Octadecyl amine polyoxyethylene ether (AC1815) has previously been used as a surface active agent and antistatic reagent (Li et al., 2013), owing to its excellent stability, emulsifiability, and susceptibility (Liang et al., 2010). Fatty amine polyoxyethylene ether has been used as mineral collector for quartz (Liu et al., 2014), kaolinite (Guo et al., 2017), and oxidized coal (Ma et al., 2018) in other literatures. In this study, AC1815 was employed as a collector for flotation separation of rutile from almandine by micro-flotation experiments. The selective adsorption mechanism of AC1815 on rutile surface was also as well investigated by zeta-potential measurements, FTIR and XPS analyses.

2. Materials and methods

2.1. Materials

The sample used in this study was the tabling concentrate obtained from Hainan, China and it contained 98% TiO_2 . The sample was ground by porcelain ball mill and screened by wet sieving, the size fraction of $-106 +48\mu m$ was obtained for the flotation experiments. On the other hand, almandine was obtained from Donghai country, Jiangsu, China. The sample was firstly processed by dry magnetic separation and vibration mill, then, the ground sample was screened by $106\mu m$ sieve. Finally, almandine single mineral within the size fraction of $-106 +48\mu m$ was obtained.

The chemical compositions of rutile and almandine samples were determined by X-ray fluorescence spectrometry (XRF) respectively, and the results are presented in Table 1. The mineral compositions of rutile and almandine were also analyzed by X-ray diffraction (XRD). The results are shown in Figs. 1 and 2.

Table 1. Chemical compositions of the rutile and almandine samples (wt%)

Composition	Na_2O	MgO	Al_2O_3	SiO_2	CaO	TiO_2	MnO	Fe_2O_3
Rutile	-	-	-	0.42	0.02	98.03	-	0.41
Almandine	0.729	5.119	17.701	38.591	9.046	1.703	0.497	26.276

2.2. Methods

2.2.1. Micro-flotation experiments

The micro-flotation experiments were carried out in a XFG- II flotation machine with a 100 cm^3 hitch groove flotation cell. The impeller speed was fixed at 1700 rpm. In single mineral flotation experiments, the mineral suspension was prepared by adding 3.0 g of single mineral to 50 cm^3 solution (6%). While in artificial mixed mineral flotation experiments, the ratio of rutile to almandine was fixed at 1:3 (0.75 g of rutile and 2.25 g of almandine). HCl and NaOH were added to adjust the pH of the suspension. After adding the desired amount of reagents, the suspension was stirred for 3 min. The skimming time was fixed at 3 min. The froth products and tailings were weighed separately after filtration and drying. The flotation recovery was calculated based on the dry weight of the products in single mineral flotation. For mixed minerals, the concentrates and tails were assayed for TiO_2 grade which was in turn used to calculate the TiO_2 recovery.

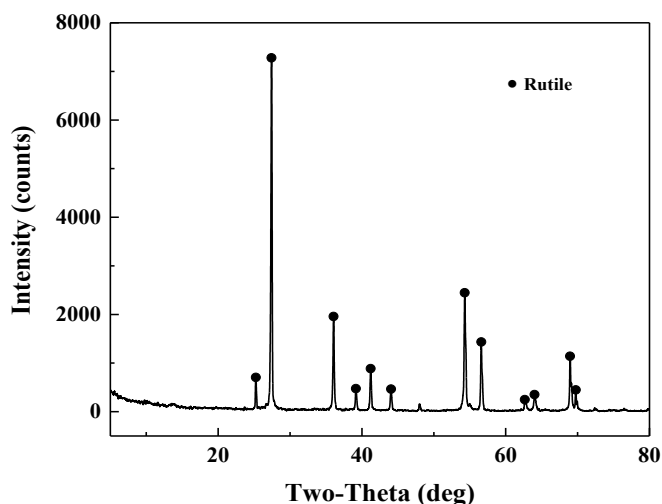


Fig. 1. XRD pattern of the rutile sample

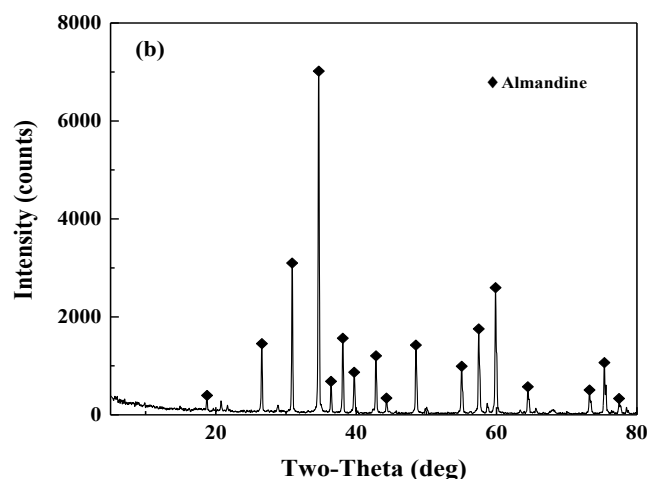


Fig. 2. XRD pattern of the almandine

AC1815 (>90 wt%) used as the collector was obtained from Haian Petrochemical factory in Jiangsu province, China (Fig. 3). The analytical grade hydrochloric acid (HCl) and sodium hydroxide (NaOH) used as pH modifiers were both purchased from Xinyang chemical reagent factory, China. Deionized (DI) water was used in the flotation and other measurements (Millipore deionized, resistivity of 18.25 M Ω ·cm).

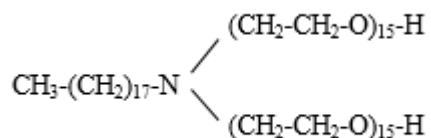


Fig. 3. Structure of collectors AC1815 (n = 15)

2.2.2. Zeta potential measurements

The zeta-potential measurements for both rutile and almandine samples were conducted with a Zetasizer Zs90 (England). The ambient temperature was maintained at 25°C, 30 mg of rutile or almandine sample (-10 μm) was added to 50 cm³ aqueous solution. This step was performed in the presence of desired reagent concentrations at a determined pH regulated through HCl or NaOH stock solutions, and the pH value recorded. The mineral suspension was magnetically stirred for 5 min and setting allowed for 10 min. Then, each sample was measured at least three times, and the average recorded as the final value (mV).

2.2.3 FTIR analysis

Fourier transform infrared (FTIR) spectra is an analytical method for determining the molecular structure of a substance and identifying compounds based on information such as relative vibrations and molecular rotations within the molecule. In this study, FTIR spectra of the samples were recorded on a Spectrum one (version BM) FT-IR(USA) spectrometer at 25°C. The interaction products were obtained in the following method. 3.0 g of single mineral sample (<37.4 μm) was added into 50 cm^3 aqueous solution with a desired reagent at pH about 6.0, after being filtered 5 min, the treated sample was washed three times with DI water, and dried in a vacuum oven at 40°C. Then, the interaction product was used for FTIR analyses.

2.2.4. X-ray photoelectron spectroscopy analysis

X-ray photoelectron spectroscopy (XPS) is an important surface analysis technique (Li et al., 2016, Liu et al., 2019). It can detect the chemical composition of the surface and depth of (<10 nm) sample. In this study, the XPS results for the samples were obtained using a Thermo Fisher ESCALAB 250 XPS system (American Thermo Fisher Scientific)

Samples for XPS measurements were prepared as follows: 3.0 g single mineral (rutile or almandine) was added into AC1815 solution with an appropriate concentration, the slurry was agitated in a flotation cell for 20 min at the speed of 1700rpm, thereafter, the slurry was filtered and dried in a vacuum oven at 60°C, the obtained products here were used for XPS analyses.

3. Results and discussion

3.1. Single mineral flotation experiments

To investigate the effect of pulp pH and AC1815 concentration on the floatability of rutile and almandine, single mineral flotation tests were conducted.

3.1.1 Effect of AC1815 dosage

Fig. 4 shows the effect of collector concentration on the recovery of rutile and almandine. As seen from Fig. 4, the floatability of rutile increases sharply from 10% to 87% up to concentration 10 mg/dm^3 with the increasing collector concentration, and then, the recovery reached a plateau to 93% at 20 mg/dm^3 collector concentration, when the concentration reaches 20 mg/L , the recovery can reach 93%. As known from the previous, when nonyl hydroxamic acid was used as a collector for rutile, the flotation recovery reached a plateau at about 85%, at a concentration was greater than 40 mg/dm^3 (Wang et al., 2016). In a similar study, when Stryl phosphonic acid (SPA) was used as a collector and sodium fluosilicate as a depressor for rutile flotation, the recovery of rutile reached about 80% only at dosages 800 g/Mg and 300 g/Mg for collector (SPA) and Sodium fluosilicate (Na_2SiF_6), respectively (Liu et al., 1999). From those previous studies reported above, then it is obvious that AC1815 shows a higher collecting performance than any other common collector. In the case of almandine, as can be seen from Fig. 4 that, while the concentration of the collector increased; especially when the concentration was lower than 10 mg/dm^3 , the recovery was below 10%. After the collector concentration was greater than 20 mg/dm^3 , the selectivity deteriorated. The results show that AC1815 is a powerful collector, and the concentration between 8 mg/dm^3 and 20 mg/dm^3 has the best selectivity for flotation separation of rutile from almandine.

3.1.2 Effect of pulp pH

Fig. 5 shows the floatability of rutile and almandine as a function of slurry pH. With the increase of the pH, the floatability of rutile increased from 22.9% at pH 2 to a maximum recovery of 95% at pH 5. When $\text{pH} > 7$, its floatability decreased significantly and reached 5% at pH 10. Compared with rutile, the floatability of almandine was relatively poor. The highest recovery was about 33% at the $\text{pH} = 6$. In the pH range of 3-7, the floatability of rutile was relatively high. Thus, good flotation selectivity could be obtained at this pH range.

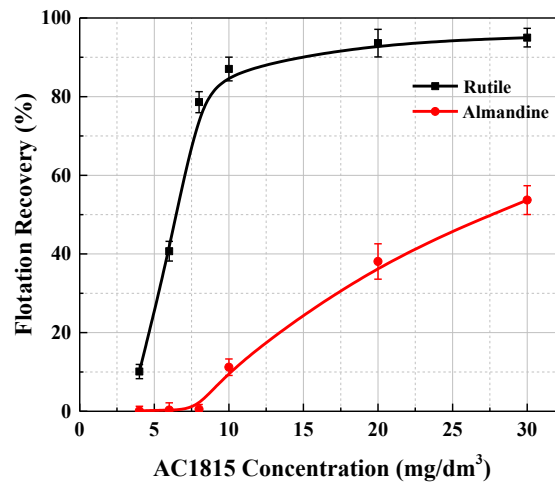


Fig. 4. Effect of AC1815 concentration on the floatability of rutile and almandine at pH=6±0.1

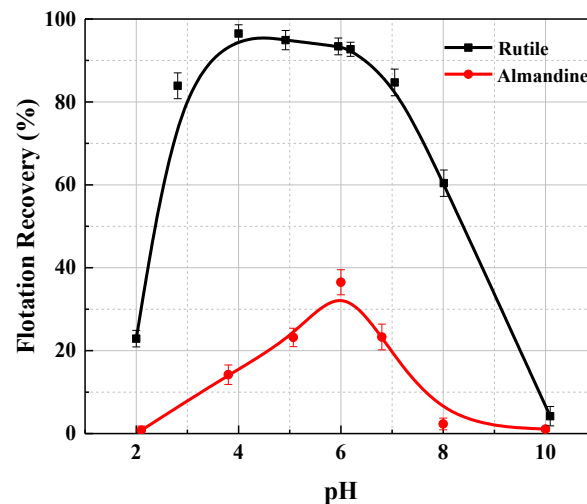


Fig. 5. Effect of pulp pH on the floatability of rutile and almandine in the presence of 20 mg/dm³ AC1815

3.2. Flotation experiments for the artificially mixed minerals

The single mineral flotation results showed that AC1815 could be a potential collector for rutile flotation. In order to investigate the flotation selectivity of AC1815 from rutile to almandine, the flotation experiments of artificial mixed minerals (the ratio of rutile to almandine was 1:3) were conducted. The effect of AC1815 concentration on the grade and TiO₂ recovery of froth concentrate are shown in Fig. 6 (pH=6) and Fig. 7 (pH=4). As seen from Figs. 6 and 7, with the increase of AC1815 concentration, the grade of froth concentrate gradually decreased, the TiO₂ recovery of froth concentrate increased significantly. In Fig. 6, when the concentration of AC1815 was 15 mg/dm³ with pH 6, then the TiO₂ grade was 41%, and the TiO₂ recovery of froth concentrate reached 90%. In Fig. 7 when the concentration of AC1815 was 8 mg/dm³ with pH 4, the TiO₂ grade was 46%, and the TiO₂ recovery of froth concentrate reached 80%. The results indicated that AC1815 could selectively separate rutile from almandine under different pH conditions.

3.3. Zeta potential measurements

Zeta potential measurement is a useful method to reveal the adsorption mechanism of reagent on minerals surfaces (Meng et al., 2015, Liu et al., 2019). The results for Zeta potentials of rutile and almandine as a function of pH are shown in Fig. 8. In the absence of AC1815, the zeta potentials of rutile and almandine decreased gradually with the increasing pH, and their isoelectric point are located at pH 1.96 and pH 3.3, respectively, which are in good agreement with previously reported studies (Liang et

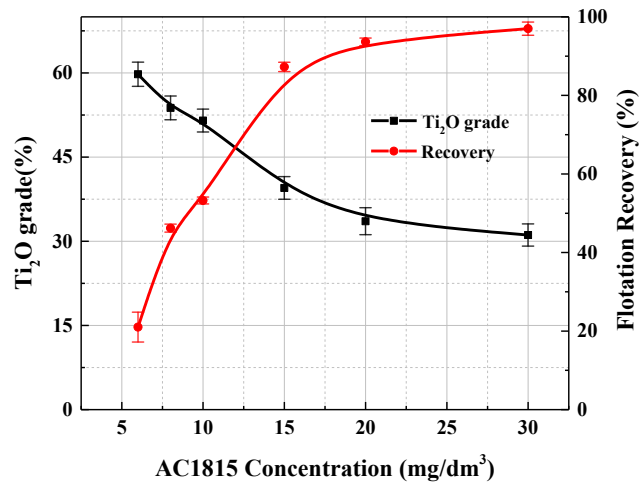


Fig. 6. Effect of AC1815 concentration on the mixed minerals flotation at pH=6±0.1

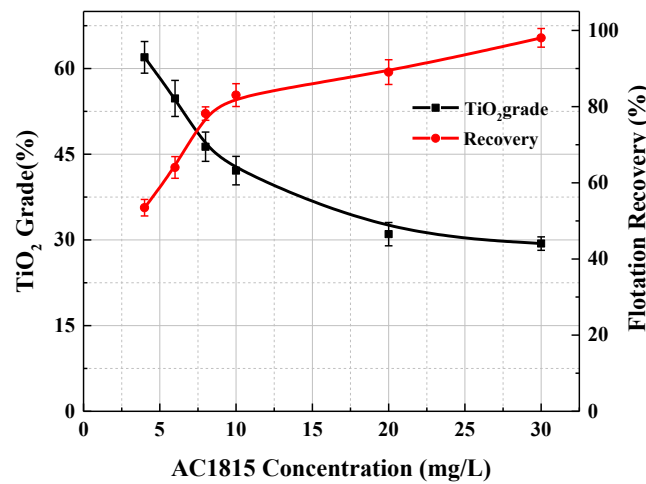


Fig. 7. Effect of AC1815 concentration on the mixed minerals flotation at pH=4±0.1

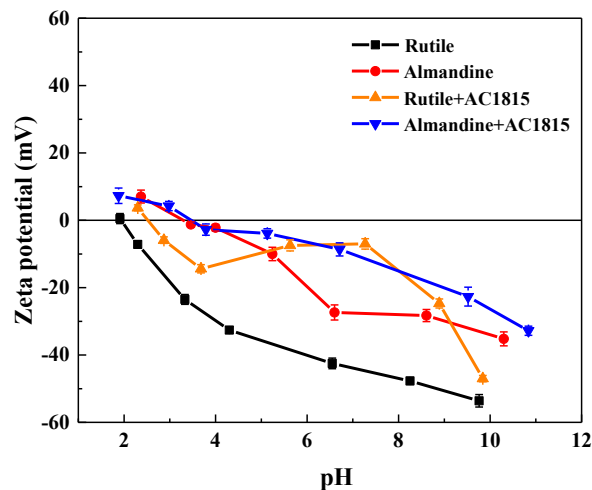


Fig. 8. Zeta potential of rutile and almandine as a function of pH in the presence of AC1815 at 20 mg/dm³

et al., 2010). After the addition of AC1815, the zeta potentials of both rutile and almandine exhibit a positive shift within the investigated pH range. The isoelectric point of rutile moved to pH 2.54 and almandine moved to pH 3.7. This might be due to the fact that the nitrogen in AC1815 has an unshared

pair of electrons, which can be protonated in a weak acid solution and form a strong electrostatic interaction with rutile and almandine surfaces, when rutile and almandine were negatively charged. The maximum variation of rutile potentials occurred in the pH range between 4 and 8 where the positive shift of potential on almandine was much smaller.

It is further noted that under the range of pH 4~8 the adsorption amount of AC1815 on rutile is larger than that of almandine, under the same pH condition of flotation experiment, therefore, the floatability of rutile is better than that of almandine with the addition of AC1815.

3.4. FTIR analyses

To investigate the type of interaction mechanism attributed to the adsorption of AC1815 on minerals' surface, FTIR analyses of rutile and almandine in the presence and absence of AC1815 were equally conducted.

In Fig. 9 the spectrum of AC1815, the characteristic peaks in the range of 4000–400 cm^{-1} were assigned based on literature (Whittaker et al., 1974, Li et al., 2013). More specifically, the bands at 2923 cm^{-1} and 2855 cm^{-1} were attributed to the stretching vibration of methyl and methylene groups ($-\text{CH}_3$ and $-\text{CH}_2-$), respectively. The peak at 1464 cm^{-1} and 1250 cm^{-1} with a relatively high intensity belongs to flexural vibration of methyl and methylene groups ($-\text{CH}_3$ and $-\text{CH}_2-$), respectively. The band at 1350 cm^{-1} and 1117 cm^{-1} comes from the symmetric stretching of C-N. The bands at 3471 cm^{-1} and 1607 cm^{-1} were attributed to the stretching vibration and deformation vibration of N-H, respectively (Chen et al., 2020). The peak at 1117 cm^{-1} and 948 cm^{-1} belong to the asymmetric stretching and symmetric stretching of aliphatic ether groups (C-O-C).

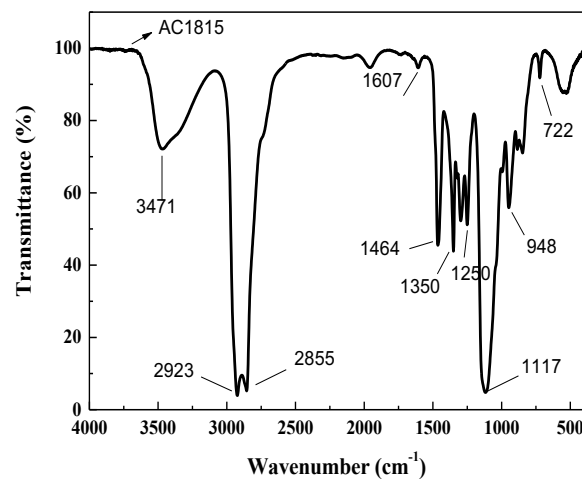


Fig. 9. The FTIR spectra of AC1815

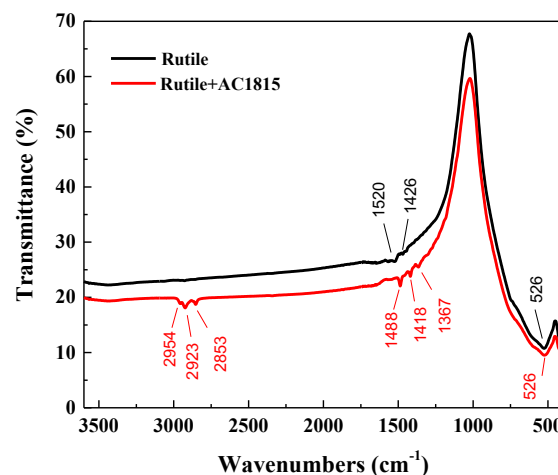


Fig. 10. The FTIR spectra of rutile before and after treatment with 20mg/dm³ AC1815

As was shown in Fig. 10, the band near 526 cm^{-1} in the spectrum of rutile in the absence of AC1815 was caused by the external bending vibration of Ti-O (Yamashita et al., 2008). Several new peaks appeared on the spectrum of treated rutile, even after three times of washing with Milli-Q water. The peak at 2954 cm^{-1} belongs to the stretching vibration of $-\text{CH}_3$, the peaks space at 2925 cm^{-1} , and 2855 cm^{-1} corresponding to the stretching vibration of $-\text{CH}_2-$, the peak at 1418 cm^{-1} belongs to bending vibrations of $-\text{CH}_2-$, the peak at 1488 cm^{-1} belongs to bending vibrations of $-\text{CH}_3$. This indicated that not just physical adsorption took place on rutile surfaces. The peak at 1367 cm^{-1} with a relatively strong intensity belongs to deformation vibration of C-N of tertiary amine (AC1815), which shifts from 1350 cm^{-1} , suggesting a hydrogen bond formed between AC1815 and rutile as well (Somasundaran et al., 1997).

Figure 11 shows the peaks at 954 cm^{-1} , 894 cm^{-1} , and 866 cm^{-1} in the spectrum of almandine which caused by the asymmetric stretching vibration of $[\text{SiO}_4]^{4+}$ groups (Yamashita et al., 2008). The peak at 634 cm^{-1} and 562 cm^{-1} with a relatively high intensity belongs to in-plane bending vibration of $[\text{SiO}_4]^{4+}$ groups. The peak at 451 cm^{-1} with a high intensity belongs to the lattice vibration of $\text{B}^{3+}-\text{O}$ ($\text{Al}^{3+}-\text{O}$ or $\text{Fe}^{3+}-\text{O}$) groups. After treated with AC1815, there were only the peaks of $-\text{CH}_3$ (2925 cm^{-1} , 1488 cm^{-1}) and $-\text{CH}_2-$ (2925 cm^{-1} , 2855 cm^{-1} and 1418 cm^{-1}) of AC1815 molecules were detected on almandine surfaces after being washed 3 times with Milli-Q water, suggesting that AC1815 molecules also adsorbed on the surface of almandine, although the interaction was relatively weaker compare to that one of rutile.

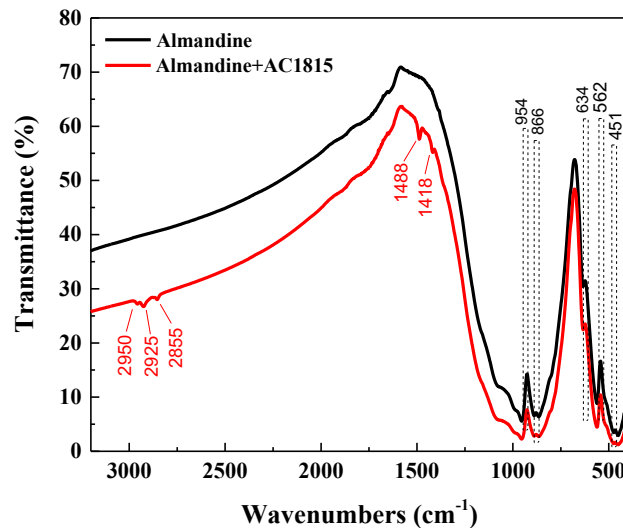


Fig.11. FTIR spectra of almandine before and after treatment with 20 mg/dm^3 AC1815

3.5. XPS analyses

XPS technique can determine the chemical states of elements, which is valuable to analyze the adsorption phenomenon on a mineral surface (Wang et al., 2015).

Figure 12 shows the survey scan of rutile and almandine before and after AC1815 treatment. On the pure rutile surface (Fig. 12a), no obvious impurities other than carbon were detected in the spectrum. After the interaction with AC1815, the intensity of the C1s peaks were slightly higher than that of the pure rutile surface. And, new peaks of N were found on rutile surface as well. The results indicated that the adsorption of AC1815 took place on the rutile surface. Figure 12b shows the survey scan of almandine before and after AC1815 treatment. After AC1815 treatment, the weak N1s XPS peaks were found on almandine surface, the intensity of the C1s peak was not stronger than that of the almandine surface.

Element compositions of rutile and almandine before and after treatment with AC1815 are given in Table. 2. As shown in Table. 2, nitrogen atoms with content of 0.89% was detected on rutile surface after treatment with AC1815, and, the content of carbon atoms on rutile surface significantly increased from 23.49% to 37.62% after treatment with AC1815. While, no nitrogen atoms were detected on almandine

surface after treatment with AC1815, and, the content of carbon atoms on almandine surface slightly increased from 24.03% to 27.78% after treatment with AC1815.

Those results of the survey scan revealed that the adsorption amount of AC1815 on rutile was obviously larger than that on almandine, thus, the good flotation selectivity could be obtained.

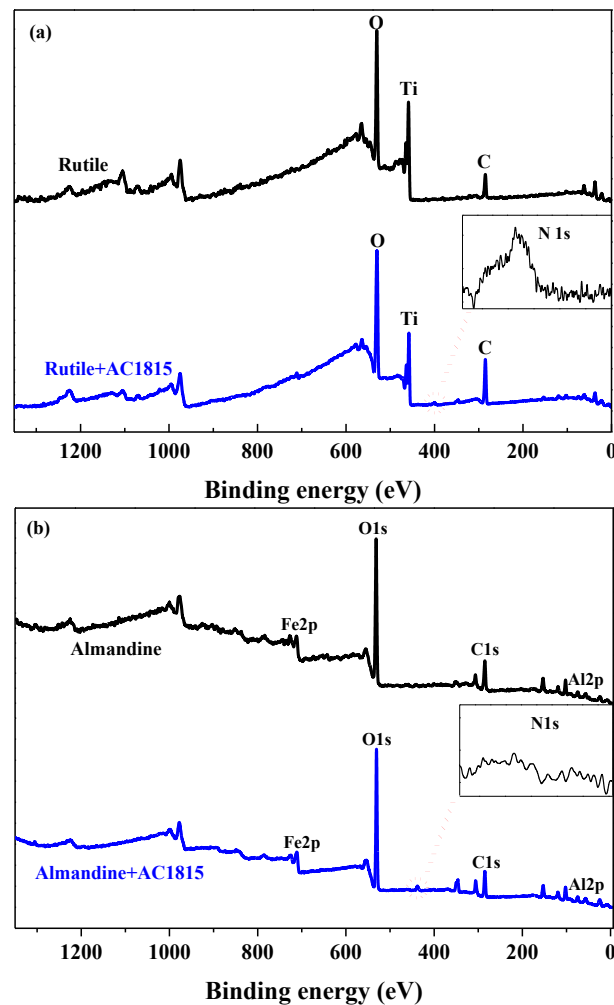


Fig.12. XPS survey scan of minerals before and after AC1815 treatment (a) rutile, (b) almandine

Table. 2. Element compositions of rutile and almandine before and after treatment with AC1815 (%)

Atomic	C1s	Ti2p	O1s	N1s	Al2p	Fe2p
Rutile	23.49	20.64	53.24	-		
Rutile+AC1815	37.62	8.29	45.48	0.89		
Almandine	24.03	-	56.82	-	8.94	5.23
Almandine+AC1815	27.78	-	44.92	-	10.45	3.20

In order to get more details for AC1815 adsorption, high resolution XPS spectra of Ti2p, O1s, C1s and N1s are exhibited in Figs. 13 and 14.

As shown in Fig. 13a, two peaks at 458.34 eV and 464.04 eV were found in Ti 2p_{3/2} and Ti2p_{1/2} emission of pure rutile sample in absence of collector (Elechiguerra et al., 2005). After the interaction with AC1815, the unchanged peaks of Ti2p indicated that no chemical bonding formed between AC1815 and rutile surface. The high-resolution O1s XPS spectra of rutile in the absence and presence of AC1815 are shown in Fig. 13b. The peak at 529.67 eV was ascribed to the lattice oxygen in crystalline TiO₂ (Yu et

al., 2005, Lin et al., 2009, Chaturvedi et al., 2017), while the other peak at 531.32eV was attributed to the surface adsorbed oxygen, such as hydroxyl species Ti-OH (Tang et al., 2018). After the interaction with AC1815, it is clearly shown that the relative intensity of -OH is more pronounced due to the C-O-C and C-OH of AC1815. The peak fit of the C1s XPS spectra of treated rutile was obtained, and shown in Fig. 13c. The C1s spectra can be well fitted with three peaks, namely 284.41 eV (C-C/C-H/CxHy)(Elechiguerra et al., 2005), 285.79 eV (C-N) (Tanget al., 2018), and 286.84 eV (C-OH) (Chen et al., 2017), indicating that hydrophilic oxygen-containing and nitrogen-containing groups were introduced on rutile surface.

In order to clearly unravel the selective adsorption mechanism of AC1815, high resolution XPS spectra of N1s is exhibited in Fig. 14. As can be seen from Fig. 14, two obvious new peaks at 399.33 eV and 401.42 eV are observed in Fig. 14a. Considering this set of data, the peak at 399.33 eV was assigned the $\equiv\text{N}$ component, hydrogen bonding interaction take place between the $\equiv\text{N}$ group of AC1815 and Ti-OH on rutile surface (Luo et al., 2018). These same references and others therein were used to locate the protonated $\equiv\text{NH}^+$ N1s signal at 401.42 eV (Benítez et al., 2011). The electrostatic interaction also took

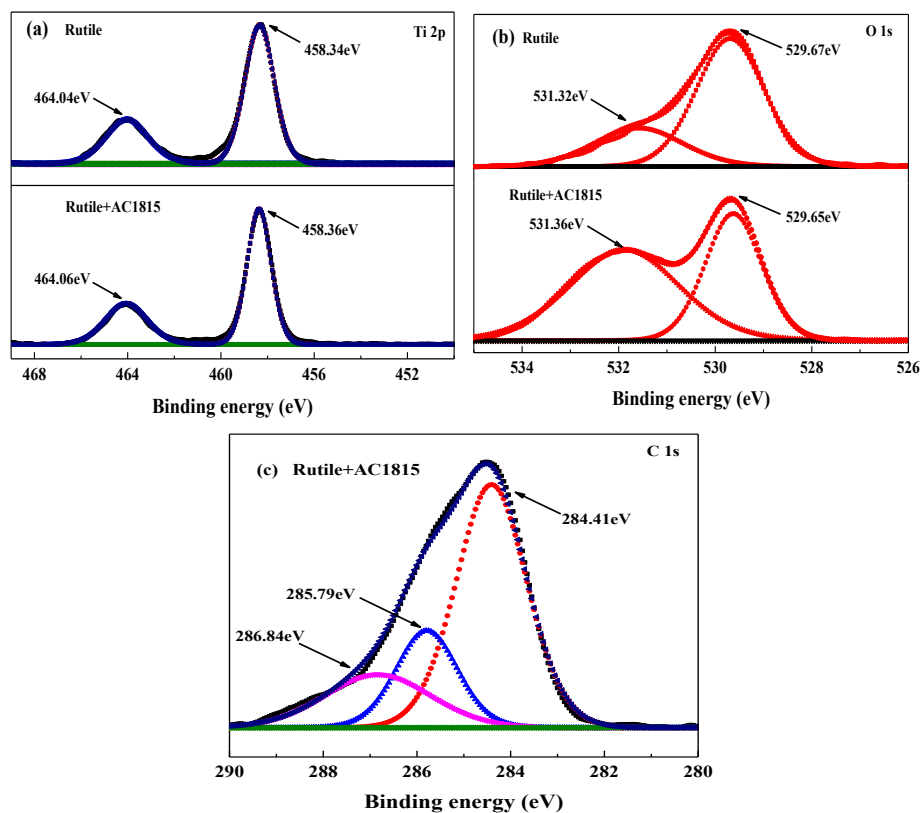


Fig. 13. Ti2p, O1s, and C1s spectra of the rutile before and after AC1815 treatment

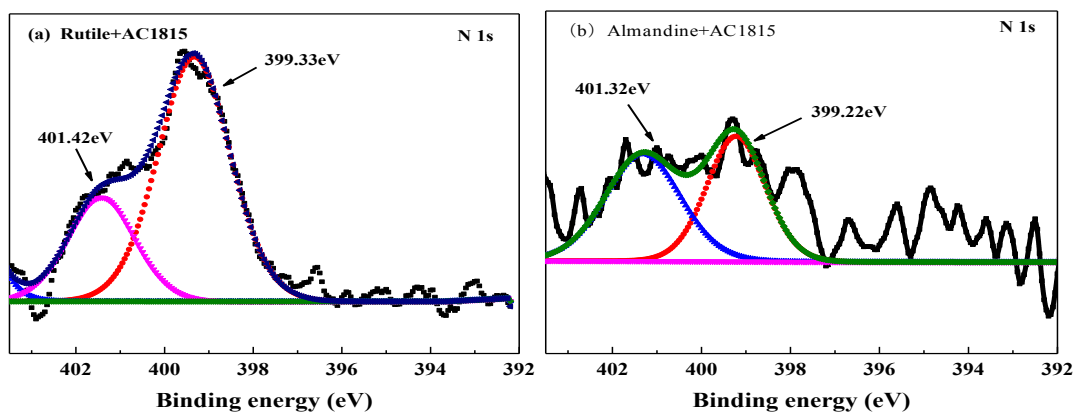


Fig. 14. N 1s spectra of minerals after AC1815 treatment (a) rutile, (b) almandine

place between the positively charged AC1815 and the negatively charged rutile surface. However, compared to that of rutile, the N1 peaks intensity of almandine was relatively weaker (Fig. 14b), indicating that less AC1815 could adsorb on almandine surface. The results are in good agreement with the zeta potential measurements.

4. Conclusions

1. The flotation results indicate that AC1815 is a powerful collector for rutile which could selectively separate rutile from almandine.
2. The zeta potential measurements revealed that positively protonated AC1815 adsorbed on rutile and almandine surface through electrostatic interaction when rutile and almandine were negatively charged.
3. FTIR and XPS analyses also indicate that the adsorption of AC1815 on rutile surface was mainly due to the electrostatic interaction, and the hydrogen bonding interaction between AC1815 and rutile. The adsorption amount of AC1815 on rutile was larger than that of almandine, thus, the good flotation selectivity could be obtained.

Acknowledgments

The financial supports for this work from the National Natural Science Foundation of China (projects No. 51974205, 51674183 and 51904208) are gratefully acknowledged. This research is also supported by the Major Scientific and Technological Innovation Project of Hubei Province (2017ACA187) and the central government guided local science and technology development projects (2019ZYYD070).

References

- ABOUZEID, A. Z. M., 1979. *Mineral processing plant design*: A.L. Mular and R.B. Bhappu (Editors). Society of Mining Engineers of the American Institute of Mining, Metallurgical, and Petroleum Engineers, Inc. New York, N.Y.
1978. *international journal of mineral processing*, 6(2),170.
- BENÍTEZ, J. J., SAN-MIGUELM. A., DOMÍNGUEZ-MEISTER, S., HEREDIA-GUERRERO, J. A., SALMERON, M., 2011. *Structure and Chemical State of Octadecylamine Self-Assembled Monolayers on Mica*. *Journal of Physical Chemistry C*, 115(40), 19716-19723.
- BERTINI, V., POCCHI, M., MARABINI, A., BARBARO, M., MUNNO, A. D., PICCI, N., 1991. *3,4-(Methylenedioxy)benzyl acrylate/acrylic acid copolymers as selective pH-controlled flocculants for finely divided titanium minerals*. *Colloids & Surfaces*, 60, 413-421.
- BULATOVIC, S., WYSLOUZIL, D. M., 1999. *Process development for treatment of complex perovskite, ilmenite and rutile ores*. *Minerals Engineering*, 12(12), 1407-1417.
- CELIK, M. S., CAN, I., EREN, R. H., 1998. *Removal of titanium impurities from feldspar ores by new flotation collectors*. *Minerals Engineering*, 11(12), 1201-1208.
- CHATURVEDI, A., JOSHI M. P., MONDAL P., SINHA, A. K., SRIVASTAVA, A. K., 2016. *Growth of anatase and rutile phase TiO₂ nanoparticles using pulsed laser ablation in liquid: Influence of surfactant addition and ablation time variation*. *Applied Surface Science*, 396, 303-309.
- CHEN, P., LI, H., SONG, S., WENG X., HE, D., ZHAO, Y., 2017. *Adsorption of dodecylamine hydrochloride on graphene oxide in water*. *Results in Physics*, 7, 2281-2288.
- CHEN, P., LIANG, Y., YANG, B., JIA, F., SONG, S., 2020. *In-situ Reduction of Au(I) for Efficient Recovery of Gold from Thiosulfate Solution by 3D MoS₂/Chitosan Aerogel*. *ACS Sustainable Chemistry & Engineering*, 8, 3673-3680.
- CHRN, Q., XU, B., ZHU, Y., LI H., CHRN, P., ZHAO, Y., LI, H., SONG, S., 2018. *Detrimental effects of slimes on the flotation of rutile from eclogite ore*. *Results in Physics*, 10, 250-255.
- CUI, L., LIU, J., 1986. *Studies on the flotation separation of rutile from garnet (in Chinese)*. *Chemical Mining Technology*, 5, 32-33.
- CUI, Z., LIU, Q., ETSSELL, T. H., 2002. *Magnetic properties of ilmenite, hematite and oil sand minerals after roasting*. *Minerals Engineering*, 15(12), 1121-1129.
- ELECHIGUERRA, J. L., LARIOS-IOPEZ, L., LIU, C., GARCIA-GUTIERREZ, D., CAMACHO-BRAGADO, A., YACAMAN, M. J., 2005. *Corrosion at the Nanoscale: The Case of Silver Nanowires and Nanoparticles*. *Chemistry of Materials*, 17(24), 6042-6052.

- FANG, S., XU, L., WU, H., TIAN, J., LU, Z., SUN, W., HU, Y., 2018. *Adsorption of Pb(II)/benzohydroxamic acid collector complexes for ilmenite flotation*. Minerals Engineering, 126, 16-23.
- Guo, L., Li, Z., Zhu, Z., Liu, Y., Fan, M., 2017. *Study and dynamics simulation of cationic collecting performance on kaolinite*. CHINA MINING MAGAZINE, 26(5), 113-116.
- LIANG, C., HAN, J., SHEN, K., 2010, *Palladium nanoparticle microemulsions: Formation and use in catalytic hydrogenation of o-chloronitrobenzene*. Chemical Engineering Journal, 165(2):709-713.
- LI, H., MU, S., WENG, X., ZHAO, Y., SONG, S., 2016. *Rutile flotation with Pb²⁺ ions as activator: Adsorption of Pb²⁺ at rutile/water interface*. Colloids and Surfaces A: Physicochemical and Engineering Aspects, 506, 431-437.
- LI, L., LIU, S., SHI, Y., YU, S., 2013. *Synthesis of terpinyl acetate using octadecylamine ethoxylate ionic liquids as catalysts*. Research on Chemical Intermediates, 39(5), 2095-2105.
- LIN, D., WU, H., ZHANG R., 2009. *Enhanced Photocatalysis of Electrospun Ag-ZnO Heterostructured Nanofibers*. Chemistry of Materials, 21(15), 3479-3484.
- LIU, A., FAN, M., 2014. *Study of Dodecyl-amine Ethoxylate Collecting Performance on Quartz*. METAL MINE, (10), 51-55.
- LIU, C., ZHU, G., SONG, S., LI, H., 2019. *Flotation separation of smithsonite from quartz using calcium lignosulphonate as a depressant and sodium oleate as a collector*. Minerals Engineering, 131, 385-391.
- LIU, C., ZHANG, W., SONG, S., LI, H., 2019. *A novel method to improve carboxymethyl cellulose performance in the flotation of talc*. Minerals Engineering, 131, 23-27.
- LIU, Q., PENG, Y., 1999. *The development of a composite collector for the flotation of rutile*. Minerals Engineering, 12(12), 1419-1430.
- LUO, B., ZHU, Y., SUN C., LI, Y., HAN, Y., 2018. *The flotation behavior and adsorption mechanisms of 2-((2-decyloxy)ethyl)amino)lauric acid on quartz surface*. Minerals Engineering, 117, 121-126.
- LI, M., QIANG, X., ZHANG, H., YAN, Z., 2015. *Synthesis and characterization of PAE-based cationic waterborne polyurethane*. Chemical Industry and Engineering Progress, 34(1), 193-197.
- Ma, Z., Li B., Guo J., Liu, S., 2018. *Effect of Nonionic Surfactants on Adsorption and Flotation Behavior of Oxidized Coal*. Coal Conversion, 163(3), 38-43.
- SOMASUNDARAN, P., KRISHNAKUMAR, S., 1997. *Adsorption of surfactants and polymers at the solid-liquid interface*. Colloids & Surfaces A Physicochemical & Engineering Aspects, 123, 491-513.
- TANG, X., YOU, Y., MAO, H., LI, K., 2018. *Improved energy storage density of composite films based on poly(arylene ether nitrile) and sulfonated poly(arylene ether nitrile) functionalized graphene*. Materials Today Communications, 17, 355-361.
- WANG, J., CHENG, H., ZHAO, H., QIN, W., QIU, G., 2016. *Flotation behavior and mechanism of rutile with nonyl hydroxamic acid*. Rare Metals, 35(5), 419-424.
- WANG, X., YU, R., WANG, P., CHEN, F., YU, H., 2015. *Co-modification of F and Fe(III) ions as a facile strategy towards effective separation of photogenerated electrons and holes*. Applied Surface Science, 351, 66-73.
- WHITTAKER E. J. W., 1974. *The Infrared Spectra of Minerals*. The Infrared spectra of minerals, Mineralogical Society.
- XIAO, W., REN, Y., YANG, J., CAO, P., WANG, J., QIN, W., QIU, G., 2019. *Adsorption mechanism of sodium oleate and styryl phosphonic acid on rutile and amphibole surfaces*. Transactions of Nonferrous Metals Society of China, 29 (9), 1939-1947.
- XIE, J., LI, X., MAO, S., LI, L., KE, B., ZHANG, Q., 2018. *Effects of structure of fatty acid collectors on the adsorption of fluorapatite (001) surface: A first-principles calculations*. Applied Surface Science, 444, 699-709.
- XU, B., LIU, S., LI, H., ZHAO, Y., 2017. *A Novel Chemical Scheme for Flotation of Rutile from Eclogite Tailing*. Results in Physics, 7, 2893-2897.
- YAMASHITA, T., HAYES, P., 2008, *Analysis of XPS spectra of Fe²⁺ and Fe³⁺ ions in oxide materials*. Applied Surface Science, 254(8), 2441-2449.
- YU, J., XIONG, J., CHENG, B., LIU, S., 2005. *Fabrication and characterization of Ag-TiO₂ multiphase nanocomposite thin films with enhanced photocatalytic activity*. Applied Catalysis B Environmental, 60(3-4), 211-221.